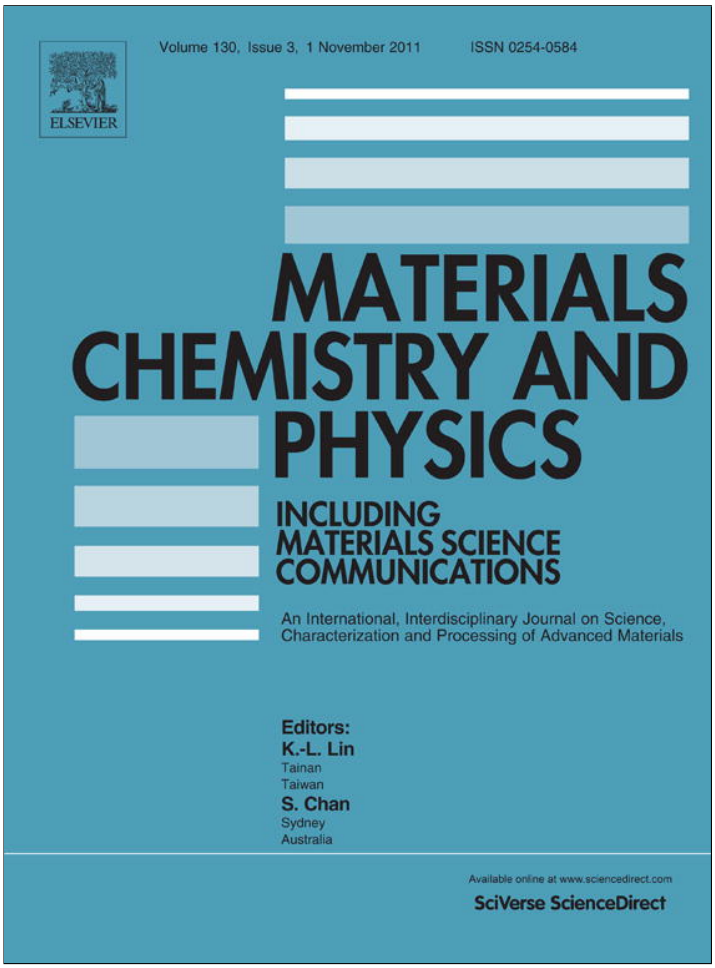

Materials Chemistry and Physics 130 (2011) 1156–1161

Contents lists available at SciVerse ScienceDirect

Materials Chemistry and Physics

journal homepage: www.elsevier.com/locate/matchemphys

Preparation of nanospinels $NiMn_xFe_{2-x}O_4$ using sol–gel method and their applications on removal of azo dye from aqueous solutions

Iman Khosravi [a], Mohammad Yazdanbakhsh [a,*], Elaheh K. Goharshadi [a,b], Abbas Youssefi [c]

[a] Department of Chemistry, Faculty of Sciences, Ferdowsi University of Mashhad, Mashhad 917791436, Iran
[b] Center of Nano Research, Ferdowsi University of Mashhad, Mashhad 91799, Iran
[c] Par -e- Tavous Research Institute, Mashhad 91000, Iran

ARTICLE INFO

Article history:
Received 28 March 2011
Received in revised form 21 August 2011
Accepted 22 August 2011

Keywords:
Nanostructures
Sol–gel growth
Thermogravimetric analysis (TGA)
Adsorption

ABSTRACT

In this paper, nanospinels $NiMn_xFe_{2-x}O_4$ ($x = 0.05$, 0.1, 0.3, 0.5, 0.7, and 1) were prepared by sol–gel method in the presence of nitrate–metal–ethylene glycol (EG) polymerized complex. The nanospinels were characterized using thermogravimetry analysis (TGA), X-ray powder diffraction (XRD), Fourier infrared spectroscopy (FTIR), and transmission electron microscope (TEM). The adsorption of an azo dye, reactive blue 5 (RB5), from water was determined using the prepared nanospinels. The effect of operational parameters such as the initial dye concentration, the concentration of nanospinels, temperature, and pH on the degradation of dye was investigated. The adsorption process follows second-order kinetics and Arrhenius behavior. Two common models, the Langmuir and Freundlich isotherms were used to investigate the interaction of dye and nanospinels. The isotherm evaluations revealed that the Freundlich model provides better fit to the experimental data than that of the Langmuir model. The photocatalytic degradation of RB5 at pH 1 under UV irradiation was examined. The results showed that the degradation of RB5 dye follows merely an adsorption process.

1. Introduction

Spinels are attractive subjects for continuous scientific interest and have been deeply investigated in material science because of their physico-chemical properties [1]. Among spinel compounds, spinel ferrites (MFe_2O_4, M=Ni, Mn, etc.) have received much research attention owing to both broad practical applications in several important technological fields such as ferrofluids, magnetic drug delivery, magnetic high-density information storages [2–10], and degradation of organic pollutants such as dyes and halogenated derivatives in wastewater treatments [11]. The textile industry uses about 10,000 different dyes and pigments and about 20–30% of total market comprises reactive dyes [12]. About 50% of initial reactive dye used in dyeing operations is released in effluents [13]. Color removal from textile wastewater is of major environmental concern because dyes create severe environmental problems by releasing toxic and potentially carcinogenic substances into the aqueous streams.

Several treatment methods including coagulation, chemical oxidation, membrane separation, electrochemical processes, and adsorption techniques have been proposed for the treatment of reactive dye wastewater. Considerable amounts of the literature reports the adsorption of dyes on various adsorbent surfaces especially nanomaterials [14,15].

The first aim of the present study is to synthesize and characterize a series of new spinel ferrite $NiMn_xFe_{2-x}O_4$ nanoparticles. Wei et al. [16] investigated the X-ray study of cation distribution in $NiMn_xFe_{2-x}O_4$ ferrites. Their compounds were not in the nano scale. Investigation of the efficiency of the spinels as adsorbents for the removal of the dye, RB5 from aqueous solutions is the second goal. Through the second goal the effect of different variables including pH, temperature, and dosage of adsorbent was evaluated. The adsorption isotherms and kinetic studies of removal of azo dye were also analyzed.

2. Experimental

2.1. Preparation of $NiMn_xFe_{2-x}O_4$ ($x = 0.05$, 0.1, 0.3, 0.5, 0.7, and 1) powders

For preparing the nanospinels $NiMn_xFe_{2-x}O_4$, proportional amounts of Fe $(NO_3)_3{\cdot}9H_2O$ (99%), Ni $(NO_3)_2{\cdot}6H_2O$ (99%), and Mn $(NO_3)_2{\cdot}4H_2O$ (99%) were dissolved in 20 ml of deionized water. 5 ml nitric acid (65%) was added to the above solution by stirring at room temperature. To make a gel, 10 ml ethylene glycol was added by stirring. The gel was heated at 80 °C for 7 h and then dried at 120 °C for 24 h. It was grounded in an agate mortar to change into a powder and fired at 750 °C in air for 4 h.

The reaction process and decomposition of the dried polymeric gel were analyzed by thermogravimetry analysis using a TGA-50 SHIMATSU from room temperature up to 1000 °C in air with a heating rate of 10 °C min^{-1}. The dried powders

* Corresponding author. Tel.: +98 511 8797022; fax: +98 511 8796416.
E-mail address: myazdan@um.ac.ir (M. Yazdanbakhsh).

0254-0584/$ – see front matter © 2011 Elsevier B.V. All rights reserved.
doi:10.1016/j.matchemphys.2011.08.048

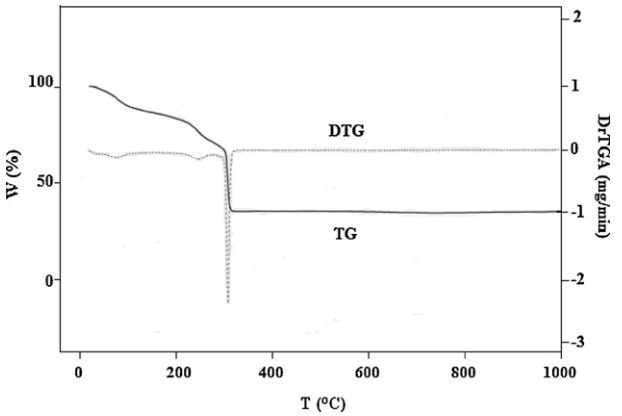

Fig. 1. TG/DTG curve of the $NiMn_{0.05}Fe_{1.95}O_4$ precursor obtained by the ethylene glycol–metal nitrate polymerized complex.

were analyzed by Fourier transform infrared spectroscopy using thermo Nicollet Nexus 870 FTIR spectrometer. The crystallization and microstructure of the oxide powders were characterized with an X-ray diffractometer employing a scanning rate of 0.02 s^{-1} in a 2θ range from 0 to 70°, using a Xî pert, 200, Philips, equipped with CuKα radiation. The data were analyzed using JCPDS standards. The morphology and dimension of the nanoparticles were observed using LEO 912 AB transmission electron microscope with the acceleration voltage of 120 kV.

2.2. Kinetic studies

The commercial color index (CI) reactive dye was used without further purification (Table 1). The initial dye concentration in each sample was 50 mg l^{-1} after adding 0.03 g of $NiMn_xFe_{2-x}O_4$ (x = 0.05 and 1) in 10 ml sample. All experiments were conducted at 25 °C. The pH was varied from 1 to 11.

Each kinetic measurement was conducted for 10 min. After a fixed time interval, the adsorbent was separated by filtration. The filtrate was analyzed spectrometrically to determine the equilibrium concentration of the dye. The absorbance of the solution was measured at 599 nm (UNICO 2800).

3. Results and discussion

3.1. Thermal analysis

Fig. 1 shows the TG/DTG curve for the nanospinel of $NiMn_{0.05}Fe_{1.95}O_4$. During the heating of the dried polymeric gel from room temperature to 1000 °C, several thermal features take place leading to a good knowledge on the reaction mechanism of spinel formation [17]. The curve shows there is three well-defined weight loss steps. At first, a continuous loss of about 10 wt.%, between room temperature and about 80 °C, takes place. Such a weight loss can be related to the drying process of the polymeric gel. At the second weight loss step (about 250 °C), a drastic weight loss of about 20% occurs. This second weight loss occurs at very narrow temperature range and it corresponds to decomposition of the organic compounds and nitrates. Then, the third weight loss step (about 315 °C), with a weight loss of about 33%, occurs during the metal–nitrate–ethylene glycol polymerized complex dried gel. Beyond the third weight loss step, temperature remains constant.

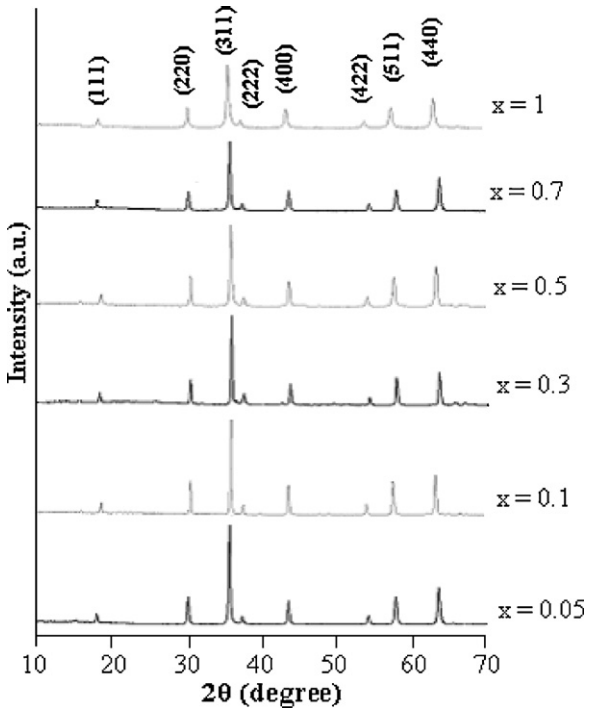

Fig. 2. XRD patterns of the $NiMn_xFe_{2-x}O_4$ powders sintered at 750 °C.

3.2. X-ray diffraction studies

Fig. 2 shows the XRD powder patterns using CuK_α radiation from the spinel-type $NiMn_xFe_{2-x}O_4$ nanoparticles. The analysis of the diffraction pattern using (1 1 1), (2 2 0), (3 1 1), (2 2 2), (4 0 0), (4 2 2), (5 1 1), and (4 4 0) reflection planes confirms the formation of cubic spinel structure of the $NiMn_xFe_{2-x}O_4$ [18,19].

Wei et al. [16] showed that with increasing Mn content, the fraction of Mn^{+3} ions in octahedral sites increases while Fe^{+3} ions in octahedral sites decreases linearly.

No secondary phase was detected in the XRD pattern which ensures the phase purity of the final products [20]. The crystallite

Table 1
Molecular structure of the studied dye.

Dye	Name	Structure	λ_{max} (nm)	M_w
RB5	Reactive Blue 5	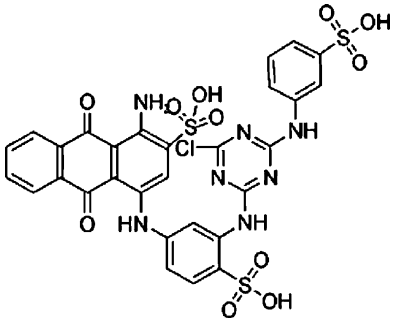	599	774.16

Table 2
The diffraction angles and lattice constants of peak (3 1 1) for all spinels $NiMn_xFe_{2-x}O_4$.

X	2θ (°)	a (Å)
0.05	35.75	8.13
0.1	35.44	8.19
0.3	35.08	8.27
0.5	34.90	8.31
0.7	34.61	8.38
1	34.20	8.48

sizes were calculated using the XRD peak broadening of the (3 1 1) peak using the Scherer's formula:

$$D_{h\ k\ l}\frac{0.9\lambda}{\beta_{h\,k\,l}\cos\theta_{h\,k\,l}} \quad (1)$$

where $D_{h\,k\,l}$ is the particle size perpendicular to the normal line of $(h\,k\,l)$ plane, $\beta_{h\,k\,l}$ is the full width at half maximum, $\theta_{h\,k\,l}$ is the Bragg angle of $(h\,k\,l)$ peak, and λ is the wavelength of X-ray. The crystallite size of nanoparticles calcinated at 750 °C is about 30 nm.

As Table 2 shows, the (3 1 1) peak shifts to small diffraction angles with the increase of Mn content and therefore the spinel with higher Mn content has a larger lattice parameter [16]. This is attributed to the different ionic radius of Mn (0.67 Å) and Fe (0.55 Å). It means that the larger the ions are the larger the resultant lattice parameter [6].

3.3. IR spectra of dried gel and annealed particles

The Far-IR spectra of all compositions were given in Fig. 3(a). The vibrations in a crystal lattice are usually observed in the range of 300–700 cm^{-1}. Two main broad metal–oxygen bands are seen in the Far-IR spectrum of all spinels and ferrites. The highest one, υ_1, is generally observed at 590 cm^{-1} which corresponds to the intrinsic stretching vibrations of the metal at the tetrahedral site (Td), $M_{Td} \leftrightarrow O$ whereas the lowest band, υ_2, is usually observed at 445 cm^{-1} which is assigned to octahedral metal stretching (Oh), $M_{Oh} \leftrightarrow O$. As Fig. 3(a) shows with the increase of Mn content, the intensity of υ_2 band increases. This is attributed to the increase of Mn^{+3} in octahedral sites [21].

The FTIR spectra (Fig. 3(b)) reveal that the vibration band of $C-O$ bond shifts from 1113 cm^{-1} for pure ethylene glycol to 1095 cm^{-1} for the current Mn-doped nickel ferrite nanocrystals which indicates that the oxygen atom of $C-O$ bond coordinates with the metal [22,23]. The surfactant molecules in the adsorbed state are influenced by the field of solid-state surface. Hence, the characteristic bands are shifted to the lower frequency regions. The surfactant molecules have strong interactions with the nanoparticles and thus it kinetically controls the growth rates of various faces of crystals and the morphology [24].

3.4. Powder morphology

As the TEM images of $NiMn_xFe_{2-x}O_4$ ($x = 0.05$ and 1) nanoparticles (Fig. 4) exhibit, the nanoparticles are in the uniformly dispersed cubic shape with an average particle size of about 28 nm.

3.5. Adsorption studies

All experiments were performed using a batch equilibrium technique placing 0.03 g of nanoparticles in a glass bottle containing 10 ml of a dye solution with 50 mg l^{-1} concentration. The separate experiments were carried out at different pH, temperatures, and adsorbent doses. The pH was adjusted with NaOH or HCl solutions using a Metrohm 620 pH meter. Here, only the results for two new nanospinels, $NiMn_xFe_{2-x}O_4$ ($x = 0.05$ and 1) are given since these are no significant difference between the results obtained for the prepared nanospinels.

3.5.1. Effect of pH

The influence of pH on the removal of azo dye by nanospinels was studied to gain farther insight into the adsorption process. To determine the optimum pH, the pH value was changed from 1 to 11 with fixed initial concentration of dye (50 mg l^{-1}) and contact time (10 min) [25]. Fig. 5 shows the percentage of removal rate of RB5 by $NiMn_xFe_{2-x}O_4$ ($x = 0.05$ and 1) nanoparticles depends strongly on pH.

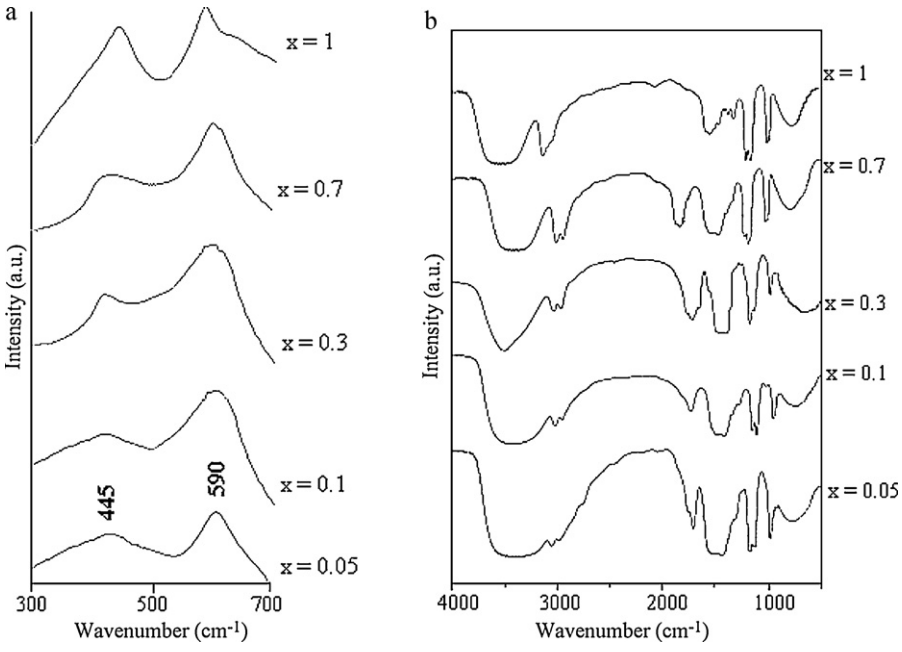

Fig. 3. (a) Far-IR spectra (b) FTIR spectra of all compositions of nanospinels $NiMn_xFe_{2-x}O_4$.

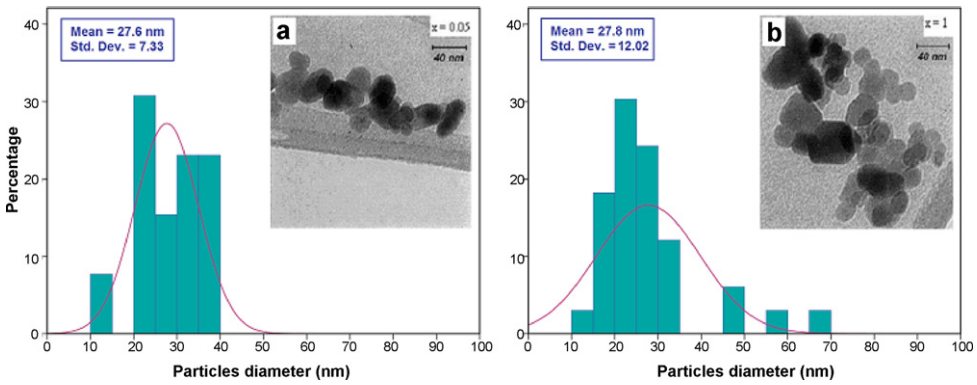

Fig. 4. TEM micrographs and calculated histograms of the $NiMn_xFe_{2-x}O_4$ for (a) $x = 0.05$ and (b) $x = 1$, polymeric gel precursors calcined at 750 °C.

The percentage of removal rate is defined as:

$$\text{Removal rate } \% = \frac{C_0 - C(t)}{C_0} \times 100 \quad (2)$$

where C_0 and $C(t)$ are the initial concentration and concentration of RB5 at time t, respectively. At pH 1, the removal of RB5 above 89% is achieved. Therefore, this pH has been selected for our next experiments.

3.5.2. Effect of temperature

The removal of RB5 by $NiMn_xFe_{2-x}O_4$ nanoparticles was carried out at 15 °C, 25 °C, 35 °C, and 45 °C. Increasing temperature from 15 °C to 45 °C leads to increase in the percentage of removal rate from 84.30 to 91, respectively. Hence, the adsorption of RB5 by $NiMn_xFe_{2-x}O_4$ nanoparticles is a kinetically controlled process.

3.5.3. Effect of adsorbent concentration

Fig. 6 shows the effect of adsorbent dosage of RB5 adsorption by $NiMn_xFe_{2-x}O_4$ nanoparticles. Because of increasing the number of binding sites, as the adsorbent dose increases, the percentage removal of dye also goes up.

3.6. Adsorption kinetics

Several models are available to investigate the adsorption kinetics. The first (Eq. (3)) and second (Eq. (4)) order reaction rate equations are the most commonly applied models [26,27]. To find a suitable chemical removal model for describing the experimental kinetic data, the data were fitted into the first and second-order models:

$$\ln C(t) = \ln C_0 - k_1 t \quad (3)$$

$$\frac{1}{C(t)} = k_2 t + \frac{1}{C_0} \quad (4)$$

where k_1 and k_2 are the first-order and second-order rate constants, respectively. The plots of experimental results of the two models showed that the removal of dye follows second-order kinetics with rate constant of 0.005 M^{-1} min^{-1}.

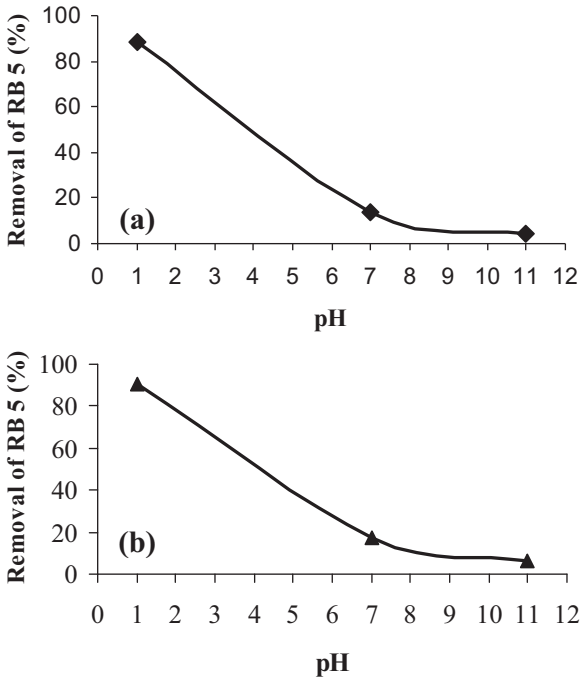

Fig. 5. Effect of pH on RB5 removal by $NiMn_xFe_{2-x}O_4$, (a) $x = 0.05$, (b) $x = 1$. Experimental conditions: mass of adsorbent, 0.03 g; initial dye concentration, 50 mgL^{-1}; volume of dye solution, 10 ml; temperature, 25 °C; time, 10 min.

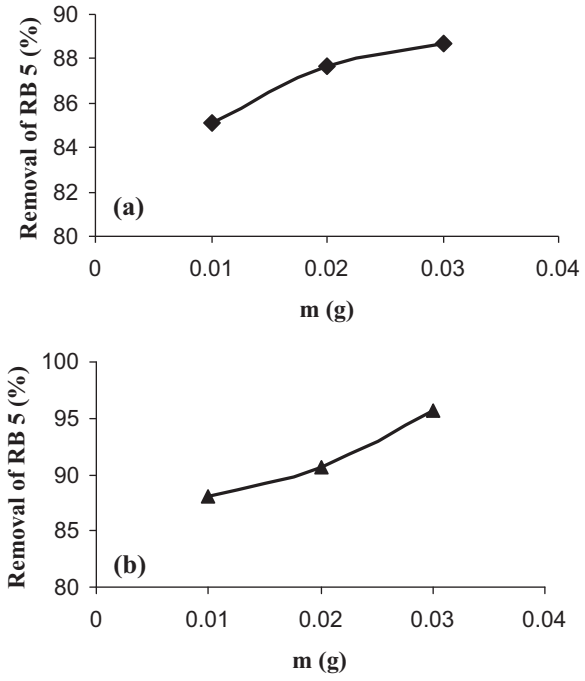

Fig. 6. Effect of adsorbent dosage of RB5 adsorption onto of $NiMn_xFe_{2-x}O_4$. (a) $x = 0.05$, (b) $x = 1$. Experimental conditions: initial dye concentration, 50 mg l^{-1}; volume of dye solution, 10 ml; temperature, 25 °C; and pH 1.

Table 3
Langmuir and Freundlich constants of RB5 adsorption over two new nanospinels.

Adsorbent	Langmuir			Freundlich		
	b (l mg^{-1})	q_m (mg g^{-1})	R^2	K_F (mg g^{-1})	n	R^2
$NiMn_{0.05}Fe_{1.95}O_4$	0.0131	212.766	0.950	0.920	1.184	0.998
$NiMnFeO_4$	0.0046	476.190	0.70	1.136	1.012	0.989

3.7. Determination of activation energy

As the removal of dye kinetics was monitored at different temperatures, the rate constants were calculated in order to find out whether the reaction follows Arrhenius behavior. According to the Arrhenius, the relationship between the rate constant of the reaction and the absolute temperature can be written as:

$$\ln k = -\frac{E_a}{R}\left(\frac{1}{T}\right) + \ln A \quad (5)$$

where k is the rate constant (M^{-1} min^{-1}), E_a is the activation energy (J mol^{-1}), R is the gas constant (8.314 J K^{-1} mol^{-1}), T is the absolute temperature (K), and A is the pre-exponential factor (M^{-1} min^{-1}). A plot of ln k versus the reciprocal of the absolute temperature should be a straight line if the reaction follows Arrhenius behavior [28]. The slope and the intercept of the line give the activation energy and the pre-exponential factor, respectively. The experimentally determined activation energy and the pre-exponential factor for $NiMn_xFe_{2-x}O_4$ ($x = 0.05$) are 0.16 kJ mol^{-1} and 0.012 $M^{-1}min^{-1}$, respectively.

3.8. Adsorption isotherms

The quantity of the dye that could be adsorbed over the nanospinels surface is a function of concentration and may be explained by adsorption isotherms. The Freundlich and Langmuir isotherm models were applied to the adsorption data. For the equilibrium concentration of adsorbate (C_e) and the amount adsorbed at the equilibrium (q_e), the following forms of the Langmuir (Eq. (6)) and Freundlich (Eq. (7)) adsorption isotherm equations were used (Eqs. (6) and (7)):

$$\frac{C_e}{q_e} = \frac{1}{bq_{max}} + \frac{C_e}{q_{max}} \quad (6)$$

$$\log q_e = \log K_F + \frac{1}{n}\log C_e \quad (7)$$

where the q_{max} (mg g^{-1}) is the surface concentration at monolayer coverage which illustrates the maximum value of q_e. The b parameter is a coefficient related to the energy of adsorption and it increases with increasing strength of the adsorption bond [29,30]. K_F and n are constants of the Freundlich equation [31]. The constant K_F represents the capacity of the adsorbent for the adsorbate and n relates to the adsorption distribution. A linear regression plot of log q_e versus log C_e gives the K_F and n values. The parameters of Langmuir and Freundlich equations for adsorption of RB5 using the $NiMn_xFe_{2-x}O_4$ ($x = 0.05$ and 1) nanoparticles were summarized in Table 3. The value of correlation coefficient for Freundlich isotherm is greater than that of the Langmuir isotherm. This indicates that Freundlich model can describe the adsorption of RB5 on nanospinels better than the Langmuir model.

3.9. Photocatalytic activity

The photocatalytic activity of $NiMn_xFe_{2-x}O_4$ ($x = 0.05$) nanoparticles for the degradation of RB5 was evaluated. In a typical experiment, 10 ml of dye solution 50 mg l^{-1} and 0.03 g of nanoparticles were mixed using a magnetic stirrer. After a period of time in the dark, the solution was irradiated. The light source was a Hg lamp (300 W, $\lambda_{max} = 365$ nm). The samples from the reaction mixture were taken from the reactor at appropriate time intervals in order to monitor the dye concentration in the solution. The solution was analyzed by the UV–vis method using UNICO 2800 spectrometer. The concentration of RB5 in the samples was calculated using the calibration curve.

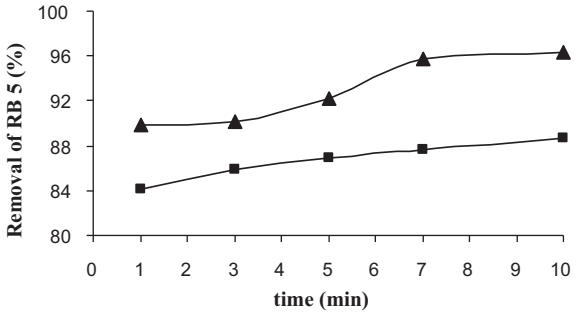

Fig. 7. The removal of RB5 (%): (■) in the present of $NiMn_xFe_{2-x}O_4$ ($x = 0.05$), without UV irradiation; (▲) in the present of $NiMn_xFe_{2-x}O_4$ ($x = 0.05$), with UV irradiation. Experimental conditions: mass of adsorbent, 0.03 g; initial dye concentration, 50 mg l^{-1}; volume of dye solution, 10 ml; temperature, 25 °C; and pH 1.

Two experiments were carried out under the same conditions, one in the presence of nanoparticles and UV irradiation and the second without UV irradiation (Fig. 7). Since some dyes are degraded by direct UV irradiation [32], it should be examined to what extent RB5 is photolyzed if no nanospinels were used. The simultaneous utilization of UV irradiation and nanoparticles increase the degradation rate of RB5 so that 90% of RB5 is removed within 1 min. In the presence of nanospinel without UV irradiation, the concentration of dye decreases quickly at the beginning, and then reaches to a saturation value as a result of adsorption of dye molecules on the nanospinel molecules. Hence, the new nanospinels cannot act as photocatalysts for the degradation of RB5 in an aqueous solution. The degradation is merely an adsorption process.

4. Conclusions

The nanoparticles $NiMn_xFe_{2-x}O_4$ ($x = 0.05$, 0.1, 0.3, 0.5, 0.7, and 1) were prepared by sol–gel method in the presence of nitrate–metal–EG agent. The XRD and TEM reveal that the nanoparticles prepared by calcinating the gel precursor at 750 °C for 4 h have good crystallinity with fine cubic spinel structure. The nanospinels exhibit regular morphology with homogeneous particle size distribution. The FTIR spectroscopy confirmed the structure of obtained nanoparticles.

In the present study, we demonstrated the nanospinels can act as novel adsorbent materials for degradation of azo dye RB5. The results demonstrated that the RB5 dye can be successfully removed from aqueous solutions by the new nanospinels. A second-order model describes the adsorption kinetic data. The equilibrium adsorption can be described using Freundlich model.

In summary, the new nanospinels are promising candidates for the adsorption of azo dyes from wastewaters.

Acknowledgments

The authors acknowledge the support of Ferdowsi University of Mashhad, Mashhad, Iran for this project (P438) and are grateful to Dr. F. Tayyari and N. Ghows for their help.

References

[1] L.K.C. De Souza, J.R. Zamian, G.N. Da Rocha Filho, L.E.B. Soledade, I.M.G. Dos Santos, A.G. Souza, Dyes Pigm. 81 (2009) 187–192.
[2] J. Amici, E. Celasco, P. Allia, P. Tiberto, M. Sangermano, Macromol. Chem. Phys. 212 (2011) 411–416.
[3] Y. Koseoglu, M. Bay, M. Tan, A. Baykal, H. Sozeri, R. Topkaya, N. Akdogan, J. Nanopart. Res. 13 (2011) 2235–2244.
[4] M. Abareshi, E.K. Goharshadi, S.M. Zebarjad, H.K. Fadafan, A. Youssefi, J. Magn. Magn. Mater. 322 (2010) 3895–3901.
[5] F. Gozuak, Y. Koseoglu, A. Baykal, H. Kavas, J. Magn. Magn. Mater. 321 (2009) 2170–2177.
[6] H. Kavas, A. Baykal, M.S. Toprak, Y. Koseoglu, M. Sertkol, B. Aktas, J. Alloys Compd. 479 (2009) 49–55.
[7] M. Han, Y. Ou, W. Chen, L. Deng, J. Alloys Compd. 474 (2009) 185–189.
[8] J. Giri, T. Sriharsha, S. Asthana, T.K.G. Rao, A.K. Nigam, D. Bahadur, J. Magn. Magn. Mater. 293 (2005) 55–61.
[9] D.E. Zhang, X.J. Zhang, X.M. Ni, H.G. Zheng, D.D. Yang, J. Magn. Magn. Mater. 292 (2005) 79–82.
[10] K.M. Wang, D.S. Lee, L. Horng, G. Chern, J. Magn. Magn. Mater. 282 (2004) 73–77.
[11] Z. Gao, F. Cui, S. Zeng, L. Guo, J. Shi, Microporous Mesoporous Mater. 132 (2010) 188–195.
[12] Z.Q. Jia, Y. Li, S. Lu, H.Z. Peng, J.Y. Ge, S.D. Chen, J. Hazard. Mater. 129 (2006) 234–238.
[13] X. Wang, N. Zhu, B. Yin, J. Hazard. Mater. 153 (2008) 22–27.
[14] M. Yazdanbakhsh, I. Khosravi, E.K. Goharshadi, A. Youssefi, J. Hazard. Mater. 184 (2010) 684–689.
[15] R. Wu, J. Qu, H. He, Y. Yu, Appl. Catal. B Environ. 48 (2004) 49–56.
[16] Q.M. Wei, J.B. Li, Y.J. Chen, Y.S. Han, Mater. Charact. 47 (2001) 247–252.
[17] X. Wei, D. Chen, W. Tang, Mater. Chem. Phys. 103 (2007) 54–58.
[18] J.L. Gunjakar, A.M. More, V.R. Shinde, C.D. Lokhande, J. Alloys Compd. 465 (2008) 468–473.
[19] G.D.C. Csete de Gyorgyfalva, I.M. Reaney, J. Eur. Ceram. Soc. 21 (2001) 2145–2148.
[20] P. Lavela, N.A. Kyerematenga, J.L. Tirado, Mater. Chem. Phys. 124 (2010) 102–108.
[21] Y. Shifeng, Y. Jingbo, Z. Enle, J. Alloys Compd. 450 (2008) 417–420.
[22] M. Sadakane, T. Horiuchi, N. Kato, C. Takahashi, W. Ueda, Chem. Mater. 19 (2007) 5779–5785.
[23] H.E. Zhang, B.F. Zhang, G.F. Wang, X.H. Dong, Y. Gao, J. Magn. Magn. Mater. 312 (2007) 126–130.
[24] M. Sertkol, Y. Koseoglu, A. Baykal, H. Kavas, A.C. Basaran, J. Magn. Magn. Mater. 321 (2009) 157–162.
[25] G. Bayramoglu, G. Celik, M.Y. Arica, J. Hazard. Mater. B 137 (2006) 1689–1697.
[26] C.L. Hsueh, Y.W. Lu, C.C. Hung, Y.H. Huang, C.Y. Chen, Dyes Pigm. 75 (2007) 130–135.
[27] D.M. Indra, C.S. Vimal, K.A. Nitin, Dyes Pigm. 69 (2006) 210–223.
[28] Z. Xiaoli, W. Jieming, W. Fengchang, W. Thanh, C. Yaqi, S. Yali, J. Guibin, J. Hazard. Mater. 173 (2010) 102–109.
[29] D.E. Kritikos, N.P. Xekoukoulotakis, E. Psillakis, D. Mantzavinos, Water Res. 41 (2007) 2236–2246.
[30] I. Langmuir, J. Am. Chem. Soc. 40 (1918) 1361–1403.
[31] H.M.F. Freundlich, Z. Phys. Chem. A 57 (1906) 385–471.
[32] I. Peternel, N. Koprivanac, H. Kusic, Water Res. 40 (2006) 525–532.